Editors' Suggestion | Featured in Physics

Observation of Magnetic Solitons in Two-Component Bose-Einstein Condensates

A. Farolfi, D. Trypogeorgos, C. Mordini, G. Lamporesi,* and G. Ferrari
INO-CNR BEC Center and Dipartimento di Fisica, Università di Trento, and Trento Institute for Fundamental Physics and Applications, INFN, 38123 Povo, Italy

(Received 22 December 2019; revised 11 February 2020; accepted 11 June 2020; published 15 July 2020)

We experimentally investigate the dynamics of spin solitary waves (magnetic solitons) in a harmonically trapped, binary superfluid mixture. We measure the *in situ* density of each pseudospin component and their relative local phase via an interferometric technique we developed and as such, fully characterize the magnetic solitons while they undergo oscillatory motion in the trap. Magnetic solitons exhibit nondispersive, dissipationless longtime dynamics. By imprinting multiple magnetic solitons in our ultracold gas sample, we engineer binary collisions between solitons of either the same or opposite magnetization and map out their trajectories.

DOI: 10.1103/PhysRevLett.125.030401

Waves have the natural tendency to spread while propagating. In nonlinear media, this tendency can be counterbalanced through a self-focusing mechanism creating localized and long-lived solitary waves, a.k.a., solitons. Their dissipationless nature makes them invaluable tools for technological applications and information transport [1,2]. They play a fundamental role across science, classical and quantum alike, and have been observed in different physical systems, such as classical fluids, liquid He, plasmas, optical waveguides, polaritons, and ultracold atomic gases [3–8]. The latter can be widely manipulated to explore soliton behavior by altering the shape of the gas, the characteristic interactions among particles, and their energy dispersion [9–18].

Two-component mixtures display an even richer excitation spectrum, showing new types of solitons. These solitons were long-sought in the liquid He community but were never observed due to the absence of an experimental realization of interpenetrable superfluids. However, mixtures of ultracold atomic gases can be used instead [19–23]. A mixture can be perturbed from its ground state by creating either excitations in the total density, with an in-phase response of the two components, or excitations in the population imbalance (magnetization), with an out-of-phase response. This implies the existence of both unmagnetized solitons, similar to those in a single component superfluid, and magnetized ones [21]. Among the latter, *magnetic solitons* (MSs) are denoted by a localized population imbalance in an otherwise balanced and symmetrically interacting mixture [24].

Atomic mixtures (superpositions) of ^{23}Na lowest-hyperfine-state atoms in the $|F, m_F\rangle = |1, \pm 1\rangle$ are fully miscible and not subject to buoyancy [25]. The two ground-state components experience the same trapping potential, show the same spatial profile, and occupy the same volume [20,22]. These are prerequisite conditions for the excitation and characterization of MSs [24], which are fulfilled in our system [20]; however, this is not the case in other atomic species, such as ^{87}Rb [21].

Here, we create MSs via spin-sensitive phase imprinting. We characterize them *in situ* using a fully tomographic method with quasiconcurrent density and relative-phase measurements that show a characteristic π jump. The MSs perform oscillatory dynamics in a harmonically confined Bose–Einstein condensate (BEC) that show only minimal dispersion and dissipation for times as long as 1 sec. In addition, we engineer collisions between MSs with same $\uparrow\uparrow$ and opposite $\uparrow\downarrow$ magnetization and monitor their behavior close to the collision point.

Experiment.—All experiments described here begin with a thermal cloud of ^{23}Na atoms in a hybrid trap [27–30] in the $|1, -1\rangle$ state, which we then transfer into an elongated crossed optical trap [Fig. 1(a)]. Further evaporative cooling leads to a BEC of typically $N \simeq 2 \times 10^6$ atoms with negligible thermal component, $T \simeq 250$ nK. The final trap frequencies are $\{f_y, f_\perp\} = \{8.7(1.2), 585(2)\}$ Hz giving axial and transverse Thomas–Fermi radii $R_y \simeq 250$ μm and $R_\perp \simeq 3.7$ μm, respectively. A uniform magnetic field is applied along the z axis with a Larmor frequency of 182.3 (1) kHz. Atoms are transferred into a mixture of $|1, \pm 1\rangle$ via a two-photon microwave radiation with an effective Rabi frequency of 268(2) Hz using an adiabatic rapid passage technique; an initially large detuning of ≈ 4 kHz is gradually reduced to zero in 60 ms [see Fig. 1(b)]. After the two-photon coupling is switched off, a dressing radiation with Rabi frequency 2.27(5) kHz is turned on, 20 kHz blue-detuned from $|1, 0\rangle \rightarrow |2, 0\rangle$, that creates an effective quadratic shift and stabilizes the mixture against spin relaxation [20,31,32].

We produce MSs by applying a steplike, purely vectorial, optical dipole potential to the right half of the BEC [Fig. 1(a)] [33]. The light is circularly polarized in order to

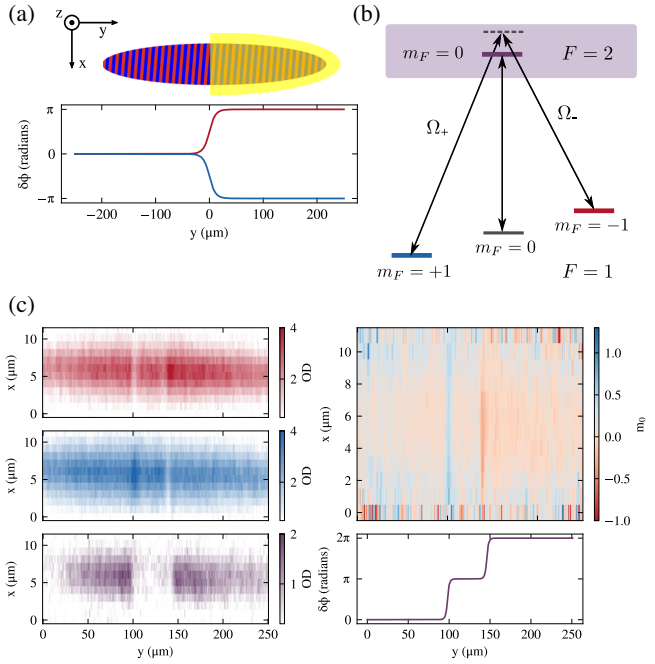

FIG. 1. (a) A spin-selective optical potential generates a pair of MSs that travel in opposite directions along y in our two-component elongated BEC. The overall imparted phase of 2π is dealt symmetrically on the two spin components. (b) Λ-coupling scheme showing all the hyperfine transitions that are used for preparation of the mixture and inducing an effective quadratic shift. (c) Full tomography of a pair of MSs 15 ms after their creation. Left column: Optical densities (OD) of $|1,-1\rangle$ (red) and $|1,+1\rangle$ (blue), and relative phase (purple). Right column: The measured apparent magnetization (top) is of the order of 0.5 and the expected relative-phase profile (bottom) shows two π jumps at the soliton positions.

maximize the vector term of the light shift and, since the atomic states have opposite angular momentum, the phase imprinted on the $|1,\pm1\rangle$ states is opposite by construction, $\phi_+ = -\phi_- = \phi/2$ [Fig. 1(a)]. Using a pulsetime of $\tau = 70$ μs, we imprint a phase of $\pm\pi$ onto the $|1,\pm1\rangle$ states. The amount of imprinted phase is independently calibrated (see Supplemental Material [35]). The phase imprint pulse does not introduce additional spin or density excitations since $\tau < h/ng \ll h/n\delta g$, where n is the total atomic density, g is the intracomponent interaction constant, δg the difference between intra- and intercomponent interactions, and h is Planck's constant. The light beam is elliptical with an aspect ratio of 5:1 and its masked intensity goes from 10% to 90% over 2 μm $\simeq 3\xi_s$, where $\xi_s = \hbar/\sqrt{2mn\delta g}$ is the spin healing length and m the atomic mass. This produces two MSs since the total magnetization of the system is conserved. They move in opposite directions, have opposite magnetization, and are robust against transverse instabilities.

The stability of a soliton depends on the ratio between its transverse extension and its thickness [36,37]. If the latter is much smaller than the former, the soliton resembles a fragile thin membrane that decays into vortical structures through snaking instability [11,16,18,38,39]. Assuming the same stability criterion valid for density solitons with the relevant quantities replaced by their spin equivalents, we expect stability for $R_\perp \lesssim 6\xi_s$. In our system $R_\perp \simeq 5\xi_s$ and the MSs show stable one-dimensional dynamics.

Time-of-flight measurements do not reveal any phase dislocations [16,38,40–42] associated with the formation of vortices or vortex rings in either component even after 1 sec from the creation of MSs (see Supplemental Material [35]). Density dynamics of the BEC are still three-dimensional, with phase coherence along the whole sample since $\mu/\hbar\omega_\perp = 9.3$, where μ is the chemical potential of the BEC.

Dynamics.—We detect the density profiles of the two components and their relative phase throughout the sample [Fig. 1(c)]. We measure density *in situ* by separately transfering 14% of the atoms from $|1,+1\rangle$ and $|1,-1\rangle$ to the $|2,0\rangle$ state and then imaging them using the $F = 2 \to F' = 3$ transition. Where one spin component shows a local density dip, the other one has a peak and vice versa. Together they comprise MSs with positive or negative magnetization, while the total density is unperturbed. The two transfers happen 600 μs apart, in which time the soliton has traversed a distance of ≈600 nm, which is smaller than our optical resolution of roughly 2 μm. After 2.5 ms, we acquire an image of the relative phase of the two components. Figure 1(c) shows a full tomographic snapshot of two MSs 16 ms after their creation at the center of the trap. They have an opposite apparent magnetization $|m_0| = |n_+ - n_-|/n = 0.5$ and have traveled to ± 20 μm with a velocity $v \simeq 1.2$ mm/s; the relative phase shows two discontinuities at these positions.

Figure 2(a) shows the MS longtime dynamics in the harmonic trap for up to 1 sec since their formation. They undergo multiple oscillations with no discernible dispersion. The oscillation amplitude is $\approx 0.4R_y$ and the period $4.7(1)T_y$, where T_y the axial harmonic oscillator period. Throughout the oscillatory dynamics we observe a slight oscillation amplitude increase and decay of magnetization, a dissipation likely induced by the residual thermal fraction, while our limited imaging resolution does not allow to observe an evolution of the width of the MS.

Varying the BEC atom number and the intensity gradient of the phase imprint light, we launch MSs with different v/c_s, where $c_s = \sqrt{n\delta g/2m}$ is the spin sound velocity. Figure 2(b) shows the dependence of the amplitude of oscillation L/R_y on the peak velocity v/c_s and is in good agreement with theory [24].

Interferometer.—We measure the relative phase of the two components using a generalized Ramsey technique. The input state of the interferometer $|1,-1\rangle + \exp\{i[\phi(y) + \phi_{\mathrm{LO}}]\}|1,+1\rangle$ is an equal superposition of the ground hyperfine levels, where, without loss of generality,

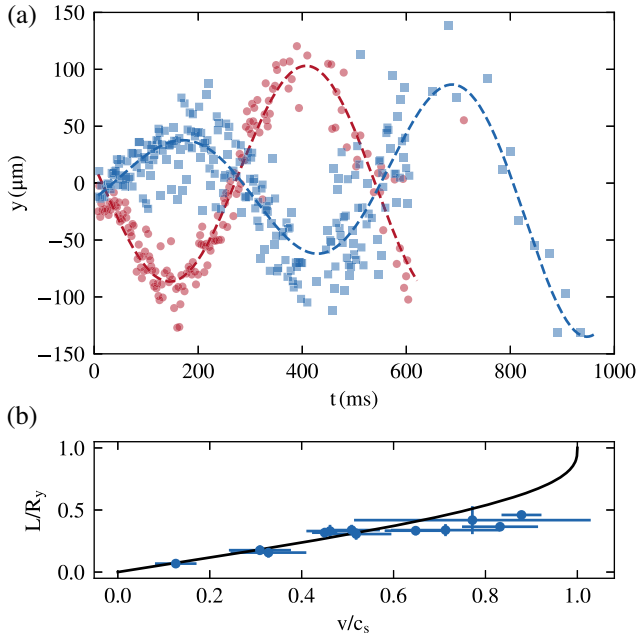

FIG. 2. (a) Two MSs of opposite magnetization oscillate out of phase in the trap with a period of 550 ms. The BEC is centered at $y = 0$. Finite temperature effects lead to the slight oscillation amplitude increase and decay of magnetization (see Supplemental Material [35]). Since the magnetization of one of the MSs is slightly smaller, it goes below our detection threshold sooner. (b) The oscillation amplitude L/R_y of a single MS increases monotonically with its initial velocity v in agreement with the theoretical prediction with no free parameters [24].

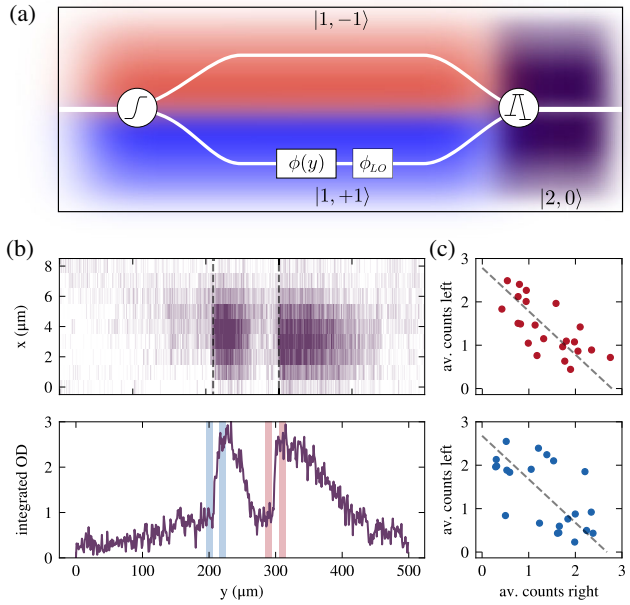

FIG. 3. (a) The input state of the interferometer is an equal superposition of the two components (red-blue). All phases are applied to one arm without loss of generality. The two components are projected onto the readout state (purple) using a bichromatic microwave pulse. (b) Typical data showing the OD in the readout state (top), which is a direct measurement of the phase difference of the two components. The jump in $\phi(y)$ is proportional to the ratio of the average counts on either side of an MS (shaded regions). (c) Average counts in the left versus right regions across each of the two MSs. The phase difference of the left- and right-projected populations is independent of ϕ_{LO}. The anticorrelated behavior is consistent with a π phase jump for both MSs within our statistical uncertainty.

the $|1, +1\rangle$ state carries all the relative phase; we ignore any global phase associated with the unitary evolution of the Hamiltonian under Larmor precession. The term $\phi(y)$ corresponds to the phase-imprint pulse, which acts locally on the BEC and initially imprints a bipartite left/right phase that is later redistributed along the BEC due to the relative motion of the MSs. The phase of the local oscillator ϕ_{LO} is the phase difference of the two microwave fields that form the interferometer and act globally on the BEC [see Fig. 3(a)]. A bichromatic microwave pulse, resonant with the $|1, -1\rangle \rightarrow |2, 0\rangle$ and $|1, +1\rangle \rightarrow |2, 0\rangle$ transitions with respective Rabi frequencies $\Omega_- = \Omega_+ = \Omega$ [Fig. 3(a)] acts as a beam splitter that projects the ground-excited-state superposition onto the population of $|2, 0\rangle$. We then image the full spatial distribution of $P_{|2,0\rangle} = \{1 + \cos[\phi(y) + \phi_{\mathrm{LO}}]\}\sin^2\Omega t$, where the populations of $|1, \pm 1\rangle$ are normalized to unity; the relative local phase of the two ground-state components is mapped onto the population of $|2, 0\rangle$. The duration of the microwave pulse is 20 μs and the two arms of the interferometer are balanced with $\Omega/2\pi = 1.12(1)$ kHz (see Supplemental Material [35]).

We are interested in how $\phi(y)$ changes across a MS. For any random ϕ_{LO}, a π jump in $\phi(y)$ results in the anticorrelated output of the interferometer when comparing the counts on the two sides of each MS. However effects such as the residual spin-dependent curvature of the potential and the excitation of long-wavelength spin waves [43,44], adversely affects the output of the interferometer. We circumvent these by restricting the phase measurement to the regions adjacent to the position of the MSs [see shaded regions in Fig. 3(b)]. Figure 3(c) shows the anticorrelation in the interferometer output channels, which appears as a distribution with -1 slope when plotted against each other.

Collisions.—We engineer ↑↑ collisions by phase imprinting two pairs of MSs in our BEC, ± 50 μm from the center, using a different optical mask. We ignore the two that travel toward the edges of the BEC and focus on the ↑↑ pair that collides at the center 45 ms later [Fig. 4(b)].

Since the size of the MSs is smaller than our optical resolution, we infer their magnetization from their velocity instead. The relative velocity of the two ↑↑MSs increases with respect to its precollision value from 1.83(8) mm/s to 2.8(1) mm/s [Fig. 4(d)], implying a change in m_0 from 0.86 to 0.62. Such a dissipative behavior is in direct contrast with the expected solitonic interactions, which are normally dissipationless. Our observations can be

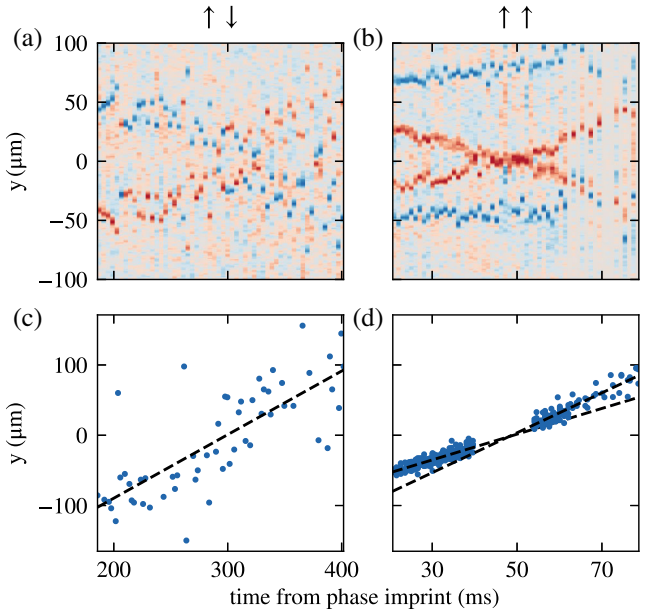

FIG. 4. Collisions of MSs with opposite (left column) or same (right column) magnetizations. (a–b) Time evolution of the MSs in the reference frame of the center of mass of the solitons. (c–d) Relative position of the MSs close to the collision point at 300 ms for ↑↓ collisions (c) and 45 ms for ↑↑ (d). For these ↑↑ collisions ($m_0 = 0.86$), the MSs dissipate energy during the collision, as evident by the different velocities (slopes) before and after. The missing points in (d) are due to not being able to distinguish same magnetization MSs when they are very close together. The variance of the data is larger in the left column than in the right one since the collision happens at much later times.

naively explained by considering that for low-magnetization ↑↑ collisions, the total magnetization at the collision is approximately the linear sum of the two MSs. However for $|m_0| > 0.5$ this would lead to magnetization larger than 1 that is unphysical. The system responds to this apparent impasse by introducing dissipation.

Collisions of MSs with opposite magnetization ↑↓ happen naturally in our system when the two MSs reach the center of the trap half an oscillation later [Fig. 2(a)]. Figure 4(a) shows their trajectories in the reference frame where the center of mass of the solitons is fixed. In ↑↓ collisions, MSs go through each other, but our signal-to-noise ratio does not allow us to conclude whether there is a change in their relative velocity [Fig. 4(c)]. The noise in ↑↓ collisions is larger than the one in ↑↑ collisions since the former happen 300 ms instead of 45 ms after the MSs' creation.

Conclusions.—We produced and characterized various aspects of MSs using the tomographic techniques described above. Our MSs are stable, nondispersive, and relatively long-lived, and their dynamic behavior is in good agreement with theory [24]. Collisions of ↑↑ solitons of large magnetization show violation of the solitonic property of nondissipative interaction. This dissipative behavior is reminiscent of light bullets: nonlinear, stable structures that appear in dispersive optical media and lose energy when they collide [45]. Our observations may trigger further studies on soliton interaction mechanisms, including the role of finite temperature effects.

With a suitable low-magnetic-field-noise environment [30,46], our techniques can be readily extended toward investigating the physics of MSs in the presence of coherent coupling between the two components [47–49]. Note that this work does not correspond to the limit of zero coupling between the two components. The solitons supported by the coupled and uncoupled systems have a distinct topological character [47,50], since the phase across a coherently coupled MS cannot be continuously unwound to $\pm\pi$.

While finalizing this manuscript, we became aware of similar work on magnetic excitations [51].

The authors are grateful to S. Stringari, F. Dalfovo, L. Pitaevskii, A. Recati, C. Qu, A. Gallemí, M. Lewenstein, and L. Tarruell for stimulating discussions. We acknowledge funding from the project NAQUAS of QuantERA ERA-NET Cofund in Quantum Technologies (Grant Agreement No. 731473) implemented within the European Union's Horizon 2020 Programme, from Provincia Autonoma di Trento, and from INFN-TIFPA under the project FISh. We thank the BEC Center and the Q@TN initiative.

*Corresponding author.
giacomo.lamporesi@ino.it; http://bec.science.unitn.it

[1] H. A. Haus and W. S. Wong, Rev. Mod. Phys. **68**, 423 (1996).
[2] M. Nakazawa, H. Kubota, K. Suzuki, E. Yamada, and A. Sahara, IEEE J. Sel. Top. Quantum Electron. **6**, 363 (2000).
[3] F. Ancilotto, D. Levy, J. Pimentel, and J. Eloranta, Phys. Rev. Lett. **120**, 035302 (2018).
[4] K. E. Lonngren, Plasma Phys. **25**, 943 (1983).
[5] T. T. Dauxois, Peyrard, and M. Michel, *Physics of Solitons* (Cambridge University Press, Cambridge, New York, 2006), formerly CIP.
[6] A. Amo, S. Pigeon, D. Sanvitto, V. G. Sala, R. Hivet, I. Carusotto, F. Pisanello, G. Leménager, R. Houdré, E. Giacobino, C. Ciuti, and A. Bramati, Science **332**, 1167 (2011).
[7] L. D. Carr and J. Brand, Multidimensional solitons: Theory, in *Emergent Nonlinear Phenomena in Bose-Einstein Condensates: Theory and Experiment*, edited by P. G. Kevrekidis, D. J. Frantzeskakis, and R. Carretero-González, Atomic, Optical, and Plasma Physics Vol 45 (Springer, Berlin, Heidelberg, 2008), pp. 133–156, https://doi.org/10.1007/978-3-540-73591-5_7.
[8] B. P. Anderson, Dark solitons in BECs: The first experiments, in *Emergent Nonlinear Phenomena in Bose-Einstein Condensates: Theory and Experiment*, edited by P. G. Kevrekidis, D. J. Frantzeskakis, and R. Carretero-González, Atomic, Optical, and Plasma Physics Vol 45 (Springer,

Berlin, Heidelberg, 2008), pp. 85–96, https://doi.org/10.1007/978-3-540-73591-5_5.
[9] S. Burger, K. Bongs, S. Dettmer, W. Ertmer, K. Sengstock, A. Sanpera, G. V. Shlyapnikov, and M. Lewenstein, Phys. Rev. Lett. **83**, 5198 (1999).
[10] J. Denschlag, J. E. Simsarian, D. L. Feder, C. W. Clark, L. A. Collins, J. Cubizolles, L. Deng, E. W. Hagley, K. Helmerson, W. P. Reinhardt, S. L. Rolston, B. I. Schneider, and W. D. Phillips, Science **287**, 97 (2000).
[11] B. P. Anderson, P. C. Haljan, C. A. Regal, D. L. Feder, L. A. Collins, C. W. Clark, and E. A. Cornell, Phys. Rev. Lett. **86**, 2926 (2001).
[12] K. E. Strecker, G. B. Partridge, A. G. Truscott, and R. G. Hulet, Nature (London) **417**, 150 (2002).
[13] L. Khaykovich, F. Schreck, G. Ferrari, T. Bourdel, J. Cubizolles, L. D. Carr, Y. Castin, and C. Salomon, Science **296**, 1290 (2002).
[14] B. Eiermann, T. Anker, M. Albiez, M. Taglieber, P. Treutlein, K.-P. Marzlin, and M. K. Oberthaler, Phys. Rev. Lett. **92**, 230401 (2004).
[15] C. Becker, S. Stellmer, P. Soltan-Panahi, S. Dörscher, M. Baumert, E.-M. Richter, J. Kronjäger, K. Bongs, and K. Sengstock, Nat. Phys. **4**, 496 (2008).
[16] I. Shomroni, E. Lahoud, S. Levy, and J. Steinhauer, Nat. Phys. **5**, 193 (2009).
[17] C. Hamner, J. J. Chang, P. Engels, and M. A. Hoefer, Phys. Rev. Lett. **106**, 065302 (2011).
[18] M. J. H. Ku, B. Mukherjee, T. Yefsah, and M. W. Zwierlein, Phys. Rev. Lett. **116**, 045304 (2016).
[19] I. Ferrier-Barbut, M. Delehaye, S. Laurent, A. T. Grier, M. Pierce, B. S. Rem, F. Chevy, and C. Salomon, Science **345**, 1035 (2014).
[20] T. Bienaimé, E. Fava, G. Colzi, C. Mordini, S. Serafini, C. Qu, S. Stringari, G. Lamporesi, and G. Ferrari, Phys. Rev. A **94**, 063652 (2016).
[21] I. Danaila, M. A. Khamehchi, V. Gokhroo, P. Engels, and P. G. Kevrekidis, Phys. Rev. A **94**, 053617 (2016).
[22] E. Fava, T. Bienaimé, C. Mordini, G. Colzi, C. Qu, S. Stringari, G. Lamporesi, and G. Ferrari, Phys. Rev. Lett. **120**, 170401 (2018).
[23] J. H. Kim, D. Hong, and Y. il Shin, arXiv:1907.10289.
[24] C. Qu, L. P. Pitaevskii, and S. Stringari, Phys. Rev. Lett. **116**, 160402 (2016).
[25] The intra- and intercomponent scattering lengths for ^{23}Na are $a = 54.54a_0$ and $a_\pm = 50.78a_0$, respectively [26], and correspond to an interaction difference $\delta a = a - a_\pm = 3.76\ a_0 = 0.07a$.
[26] S. Knoop, T. Schuster, R. Scelle, A. Trautmann, J. Appmeier, M. K. Oberthaler, E. Tiesinga, and E. Tiemann, Phys. Rev. A **83**, 042704 (2011).
[27] G. Lamporesi, S. Donadello, S. Serafini, and G. Ferrari, Rev. Sci. Instrum. **84**, 063102 (2013).
[28] G. Colzi, G. Durastante, E. Fava, S. Serafini, G. Lamporesi, and G. Ferrari, Phys. Rev. A **93**, 023421 (2016).
[29] G. Colzi, E. Fava, M. Barbiero, C. Mordini, G. Lamporesi, and G. Ferrari, Phys. Rev. A **97**, 053625 (2018).
[30] A. Farolfi, D. Trypogeorgos, G. Colzi, E. Fava, G. Lamporesi, and G. Ferrari, Rev. Sci. Instrum. **90**, 115114 (2019).
[31] F. Gerbier, A. Widera, S. Fölling, O. Mandel, and I. Bloch, Phys. Rev. A **73**, 041602(R) (2006).
[32] K. Jiménez-García, A. Invernizzi, B. Evrard, C. Frapolli, J. Dalibard, and F. Gerbier, Nat. Commun. **10**, 1422 (2019).
[33] We set the scalar part of the potential equal to zero by an appropriate choice of the laser frequency $\lambda = 589.557$ nm, which is detuned to the blue of the $3^2S_{1/2} \rightarrow 3^2P_{1/2}$ ^{23}Na transition and to the red of the $3^2S_{1/2} \rightarrow 3^2P_{3/2}$ transition [34].
[34] R. Grimm, M. Weidemüller, and Y. B. Ovchinnikov, Adv. At. Mol. Opt. Phys. **42**, 95 (2000).
[35] See Supplemental Material at http://link.aps.org/supplemental/10.1103/PhysRevLett.125.030401 for details on detection and decay of MS, phase imprint calibration and spin sound excitations.
[36] J. Brand and W. P. Reinhardt, Phys. Rev. A **65**, 043612 (2002).
[37] S. Komineas and N. Papanicolaou, Phys. Rev. A **68**, 043617 (2003).
[38] C. Becker, K. Sengstock, P. Schmelcher, P. G. Kevrekidis, and R. Carretero-González, New J. Phys. **15**, 113028 (2013).
[39] A. Muñoz Mateo and J. Brand, Phys. Rev. Lett. **113**, 255302 (2014).
[40] M. J. H. Ku, W. Ji, B. Mukherjee, E. Guardado-Sanchez, L. W. Cheuk, T. Yefsah, and M. W. Zwierlein, Phys. Rev. Lett. **113**, 065301 (2014).
[41] S. Donadello, S. Serafini, M. Tylutki, L. P. Pitaevskii, F. Dalfovo, G. Lamporesi, and G. Ferrari, Phys. Rev. Lett. **113**, 065302 (2014).
[42] M. Tylutki, S. Donadello, S. Serafini, L. Pitaevskii, F. Dalfovo, G. Lamporesi, and G. Ferrari, Eur. Phys. J. Special Topics **224**, 577 (2016).
[43] C. Hamner, Y. Zhang, J. J. Chang, C. Zhang, and P. Engels, Phys. Rev. Lett. **111**, 264101 (2013).
[44] Note, for instance, the difference between Fig. 1(c) lower panel and Fig. 3(b) top panel, which, despite being taken in similar experimental settings, show a qualitatively different pattern. From single magnetization images of atomic clouds with a much larger aspect ratio 100∶1, we estimate the energy curvature to be 450 Hz/mm^2, or 28 Hz for our $R_y = 250\ \mu$m BEC.
[45] C. Milián, Y. V. Kartashov, and L. Torner, Phys. Rev. Lett. **123**, 133902 (2019).
[46] D. Trypogeorgos, A. Valdés-Curiel, N. Lundblad, and I. B. Spielman, Phys. Rev. A **97**, 013407 (2018).
[47] C. Qu, M. Tylutki, S. Stringari, and L. P. Pitaevskii, Phys. Rev. A **95**, 033614 (2017).
[48] S.-W. Su, S.-C. Gou, A. Bradley, O. Fialko, and J. Brand, Phys. Rev. Lett. **110**, 215302 (2013).
[49] S. S. Shamailov and J. Brand, SciPost Phys. **4**, 18 (2018).
[50] J. Sanz, A. Frölian, C. S. Chisholm, C. R. Cabrera, and L. Tarruell, arXiv:1912.06041.
[51] X. Chai, D. Lao, K. Fujimoto, R. Hamazaki, M. Ueda, and C. Raman, following Letter, Phys. Rev. Lett. **125**, 030402 (2020).